university of groningen / faculty of science and engineering

Draft version July 4, 2024
Typeset using LaTeX **twocolumn** style in AASTeX631

The star formation histories of Lyman-alpha emitters at $z = 3 - 7$

BSc Thesis

Daniil Ceban, s4642260, d.ceban@student.rug.nl

Supervisors: Prof. Karina Caputi & Dr. Edoardo Iani
Second Reader: Dr. Gijs Verdoes Kleijn

ABSTRACT

Problem definition: Ly-α emitting galaxies (LAEs) are usually detected via their intense UV emission lines, which are known to trace young stars. Thus, LAEs are generally considered blue, low-mass objects. However, recent studies have revealed the presence of an underlying older population in a significant fraction of these objects ($\approx 30\%$), suggesting that some LAEs might be rejuvenating rather than exclusively young, which raises a question about their true star formation histories and evolution.

Methods: We consider a sample of 182 Ly-α emitters detected in the eXtreme Deep Field (XDF) at $z \approx 3 - 7$. Using robust photometry consisting of 27 bands provided by both HST and JWST, we perform spectral energy distribution (SED) fitting using Code Investigating GALaxy Emission (CIGALE). We examine the stellar population properties across four star formation history (SFH) types: exponential decline, and delayed exponential with no burst, mandatory burst or optional burst in star formation. We compare the resulting physical properties (Age, M_*, SFR) and discuss the implications in the context of the relative placement of our LAEs along the main-sequence of star-forming galaxies.

Results: Across all models, we find a consistent fraction of young (≤ 100 Myrs) LAEs, constituting roughly 80% of the sample. When no burst is included, young LAEs are mostly low-mass systems with high star formation rates, leading to a clear specific star formation (sSFR) bimodality between young and older (> 100 Myrs) objects. As a result, young LAEs reside in the starburst region of SFMS. However, incorporating a bursty SFH shows that 85% of our LAEs tend to fit a recent burst, blurring the age distinction and reducing the degree of starburst trend among young LAEs. However, our χ^2 analysis shows no preference towards either SFH.

1. INTRODUCTION

1.1. *LAEs*

Lyman-α (Lyα) emitters, otherwise known as LAEs, are galaxies detected thanks to their prominent Ly-α emission line. This emission line corresponds to a 121.6 nm photon emitted during a hydrogen electron transition from the first excited state down to the ground state, which is why it is often associated with active star formation. O and B stars ionize the interstellar medium and excite surrounding hydrogen atoms, resulting in the

characteristic UV emission when the hydrogen later recombines.

At large distances, this rest-frame UV emission is shifted into the optical part of the spectrum due to the effect of cosmological redshift. This, combined with Ly-α being the brightest hydrogen transition, results in most LAEs being detected at $z \geq 3$, making them perfect tools for studying the early universe up to the epoch of reionization. During periods of high HI abundance, the universe was opaque to these photons due to their short wavelength. However, as the medium became more ionized, the optical depth decreased, allowing the detection of Ly-α line (Finkelstein 2016; Ouchi et al. 2020). Thus, by observing the variation of Ly-α emission as a function of redshift, one can trace the evolution of neutral hydrogen distribution across cosmic time.

Due to their high redshift, LAEs have been traditionally characterized as very young, low-mass systems with intense star formation (Ouchi et al. 2020). However, recent studies have presented convincing evidence of an old underlying stellar population in some LAEs, which was previously undetected due to the low spacial resolution and shallow observation depth available in the rest-frame optical/NIR regions of such galaxies (Finkelstein et al. 2009; Iani 2024). These results raise doubts about whether LAEs are truly young or are merely experiencing a rejuvenation phase (Rosani et al. 2020). Consequently, in this work, we aim to constrain the star formation histories of LAEs in an attempt to uncover more information regarding their evolution.

1.2. *Spectral energy distribution*

Spectral energy distribution (SED) fitting is a method used to infer physical properties of galaxies by observing the intensity of their radiation at different wavelengths. The idea behind this technique lies in the fact that various processes throughout a galaxy's lifetime have produced radiation in associated wavelengths, and from a multi-wavelength study one could backtrack the evolution of a galaxy and infer its current state. Naturally, the best results would then be obtained for a larger number of observed filters and wider wavelength coverage, while more constricted observations would require the code to make numerous assumptions about the data (Conroy 2013, for a deeper discussion see Section 4).

A number of codes were designed to untangle this by pre-computing a large number of galaxy models and comparing them to the observed spectrum. In that way, the physical properties that went into creating the best fitting model would be assigned to the observed galaxy. However, there are always prior assumptions the user has to make before the models can be computed, mostly involving the adopted star formation history (SFH), initial mass function (IMF), metallicity evolution and other variable parameters. Therefore, the fitting outcome can drift depending on the prior, with the SFH often causing some of the most significant discrepancies (Maraston et al. 2010; Pacifici et al. 2015).

We will explore this further by analyzing our LAE sample using the Code Investigating GALaxy Emission (CIGALE, Boquien et al. 2019). We choose this software due to the flexibility it allows in terms of handling various SFH types, as well as in modelling of emission lines and dust attenuation which is well suited for galaxies such as ours. Unlike many similar codes, CIGALE does not compute the best-fit model on a grid, with the authors opting towards Bayesian style estimation instead. That is to say, all models are weighted by their quality of fit thereby incorporating the uncertainty information into the final result. The same approach can also be applied to the best-fit physical parameters, which helps avoid binned outputs.

This thesis is organised as follows: In Section 2, we outline the origin of our dataset and describe the prior knowledge we have concerning some of the properties of those LAEs. In Section 3, we explain the procedure of SED fitting for various SFH models and analyze the outcome. We discuss the quality of fit of each SFH, and interpret the discrepancies in the main physical parameters or lack thereof. We conclude the section by placing our LAEs on the SFR-M_* plane and considering the implications. Finally, in Section 4 we explore the significance of particular bands in our photometry, focusing on the importance of combining HST data with JWST as well as the impact of mid-band photometry.

In our work, we assume $\Omega_M = 0.3$, $\Omega_\Lambda = 0.7$, and $H_0 = 70$ km s^{-1}Mpc^{-1}. All magnitudes are in the AB magnitude system (Oke & Gunn 1983), and all times refer to the time since the beginning of the Universe at given redshift. We assume a Chabrier (2003) IMF.

2. DATA SET

Our work is based on a set of 182 LAEs in the $z \approx 3-7$ redshift range obtained by Iani (2024). This chapter is meant to provide context surrounding the detection procedure and selection criteria, and we stress that this is merely a summary and none of the steps outlined below were done as a part of this project.

The initial observations were made in the Hubble eXtreme Deep Field (XDF, Illingworth et al. 2013) - a region of space where the deepest Hubble Space Telescope (HST) imaging has ever been attained. The Multi

Unit Spectroscopic Explorer (MUSE, Bacon et al. 2010, 2023) from VLT (Very Large Telescope) provided detailed spectra of objects in the area, allowing the detection of LAEs through their strong Ly-α emission line and measuring their corresponding redshifts.

The spectroscopy was complemented by imaging, both from HST (WFC3 & ACS) as well as JWST (MIRI & NIRCam). JWST images were compiled from a number of sources: the mid-band imaging data was taken from JWST Extragalactic Medium-band Survey (JEMS, Williams et al. 2023) and The First Reionization Epoch Spectroscopic COmplete Survey (FRESCO, Oesch et al. 2023), while images in wide bands were obtained from The JWST Advanced Deep Extragalactic Survey (JADES, Rieke et al. 2023). This imaging data was combined with HST observations from the Hubble Legacy Field GOODS-S (HLF-GOODS-S, Whitaker et al. 2019), which were taken in 13 various filters spanning a range of wavelengths from UV to NIR. All images were processed adequately, reducing artifacts to a minimum and aligning the results to the same pixel scale (Bagley et al. 2023; Pérez-González et al. 2024).

With the data being obtained and LAEs identified from MUSE catalogue (Bacon et al. 2023), a selection procedure followed to ensure data quality of the initial sample of LAEs. First, objects with a low confidence in redshift estimation were discarded, later followed by sources bordering galaxies bright enough to potentially pollute the spectrum. Subsequently, the presence of both Type I and Type II AGN was ruled out by matching the LAEs with the available catalogues of known AGNs in the XDF, both by confirming a lack of prominent X-ray emission (Ranalli et al. 2013; Luo et al. 2017; Evans et al. 2020), as well as characteristic emission lines in other wavelengths (Lyu et al. 2022; Bacon et al. 2023). These preemptive steps resulted in a sample narrowed down to 450 Ly-α emitters.

Lastly, the HST/JWST counterparts of the LAEs had to be identified. Since a clear identification is challenging due to scattering and a rough PSF, the following procedure was adopted: a catalogue was created using SExtractor (Bertin & Arnouts 1996), providing photometry for all sources in all HST & JWST filters used. Errors were propagated accounting for possible underestimation by the software (Sonnett et al. 2013), and non-detections in a given filter were superseded by upper limits. This catalogue was then used to conduct SED fitting using LePHARE (Ilbert et al. 2006), allowing the code to fit redshift as a free parameter. The photometric redshifts of possible counterparts were then compared to those of the Ly-α emitters, and catastrophic outliers were discarded, leaving only the most likely counterparts. Subsequently, LAEs with multiple counterparts or emission sources were discarded to prevent misidentification and ensure a meaningful interpretation of their physical parameters. As a result, 250 LAEs were matched with a counterpart, 182 of which with a singular one. These 182 LAEs mark the end of sample selection and constitute our final selected data set.

We possess the photometry of each object in 27 filters from both HST and JWST, covering a wavelength interval $\lambda \approx 0.2 - 5.6\mu m$. The large number of data points and broad range of wavelengths spanned by these instruments provide us with a strong base for subsequent analysis of these LAEs.

3. RESULTS AND ANALYSIS

3.1. *SED fitting*

3.1.1. *Fitting parameters*

In this work, we are using CIGALE (Boquien et al. 2019) as our main fitting tool. Throughout the procedure, we will assume the stellar population synthesis model proposed by Bruzual & Charlot (2003) based on a Chabrier IMF (Chabrier 2003). This combination is preferred for high-redshift low-mass systems such as LAEs due to an increased wavelength coverage and spectral analysis resolution of the single stellar populations (SSPs), as well as Chabrier IMF's capability to reliably generate lower-mass objects. Given that LAEs are known to have low metallicity (Finkelstein et al. 2011; Yuan et al. 2013; Ouchi et al. 2020), we allow the code to span only solar and subsolar metallicities and restrict it to $0.0001 \leq Z \leq 0.02$.

Since Bruzual & Charlot SSP models include pure stellar populations without considering nebular emission, they need to be combined with a photoionization code if one is to accurately model star forming galaxies. Therefore, we enable the code to fit emission lines and complement the model with the attenuation law proposed by Calzetti et al. (2000), which will affect both the emission lines as well as the generated stellar populations. We allow the colour excess of the nebular lines to range from 0.01 to 0.5 in increments of 0.1, with the upper limits chosen for consistency with previous findings (Ono et al. 2010; Ouchi et al. 2020). The attenuation of the stellar continuum will be assumed equal to the one of nebular lines.

For star formation histories, we test two main parametrisations:

1. An exponentially declining SFH (SFR(t)$\propto e^{-\frac{t}{\tau}}$) for $0 \leq t \leq t_0$, where t_0 is the lookback time to the beginning of star formation, and τ is the characteristic e-folding time.

2. A delayed SFH (SFR(t)$\propto \frac{t}{\tau^2}e^{-\frac{t}{\tau}}$), where τ functions as both the time at which the star formation peaks as well as the e-folding time of the decline after the peak.

For those cases, CIGALE is allowed to fit the age of the main stellar population ranging from 2 Myrs to 1 Gyr, with τ values spaced out from 1 Myr to 1.5 Gyr. It is important to note that choosing an exponentially declining SFH is not an option directly available in CIGALE. It was created by choosing a periodic exponential SFH and setting the time between the beginning of each iteration equal to the age of the universe, effectively restricting the SFH to one exponential period.

Additionally, we investigate the implications of a recent burst by adding a period of constant star formation to the delayed SFH. The burst is modeled as a constant term added to the SFH, with a specific value set for its e-folding time much larger then its age to prevent folding. With the burst, we focus on two cases: one with a mandatory burst (mass fractions 0.01, 0.1, 0.3, 0.5, 0.7, or 0.99) and one with an optional burst (same fractions with a possibility to also choose 0). In this case, the burst fraction is defined as a fraction of total stellar mass of the galaxy which is contained within the recent burst(Boquien et al. 2019; Boquien M., private communication). We show a sample SFH of each type in Figure 1. Since the assumption of a constant star formation is not reliable on longer timescales, we restrict the burst to be up to 15 Myrs old, automatically imposing a numerical restriction which prevents the main stellar population from being of the same age or younger.

3.1.2. *Star formation rates*

It is generally known that SFR determined from SED fitting can be unreliable. Inconsistency can arise due to numerical effects such as the chosen SFH or degeneracy with dust attenuation (Boquien et al. 2014; Haskell et al. 2024), or individual assumptions within a particular fitting code (see Hunt et al. 2019; Pacifici et al. 2023). Thus, to minimize software biases and maintain consistency with the literature, we will estimate SFR empirically.

We derive the star formation rates from UV rest-frame magnitude of our LAEs. It is important to note that various empirical estimates result in SFR over different timescales, with M(UV) indicating SFR averaged over the past $\approx$ 100 Myrs (Kennicutt & Evans 2012; Calzetti 2013; Sparre et al. 2017).

As a first step, we determine which photometric filters cover the rest-frame wavelength of 1500 Å for each object (Rodrigo & Solano 2020). If no filters span the needed wavelength, we take the magnitude of the closest one instead; if more then one filter covers the range, we take their average magnitude. This process is repeated for every wavelength in the 1500-2500 Å range in steps of 10 Å, and the biweght location of the result provides our best estimate for UV apparent magnitude of each object.

Subsequently, the obtained apparent magnitudes are converted to absolute using the distance modulus:

$$M = m - 5\ \log\left(\frac{d_L}{10}\right) + 2.5\ \log(1+z) - A(\lambda) \quad (1)$$

where d_L is luminosity distance in pc obtained from the redshift value. The last term is required for dust correction, where we follow the prescription of Calzetti et al. (2000) and subtract the term $A(\lambda) = E(B-V)\ k(\lambda)$, with $k(\lambda)$ being the starburst reddening curve taken in the interval 0.12 - 0.63 μm.

As per Iani (2024), we proceed to convert the dust-corrected M(UV) into monochromatic luminosity using

$$L_\nu = 10^{-0.4(M(UV)-51.6)} \quad (2)$$

and then to SFR (Kennicutt 1998):

$$\mathrm{SFR}(M_\odot/\mathrm{yr}) = 0.63\times1.4\times10^{-28}L_\nu\ (\mathrm{erg\ s^{-1}Hz^{-1}}) \quad (3)$$

The 0.63 factor correction is required to account for the assumption by Kennicutt of a Salpeter IMF (Salpeter 1955) as opposed to Chabrier IMF used in this work (see Madau & Dickinson 2014). This step finalizes the procedure and provides our final SFR estimates from UV magnitude.

3.2. *Comparing single and composite SFH*

We now run CIGALE for each of the 4 SFH models, and extract the estimated physical parameters. However, in order to arrive to any meaningful conclusions, we first need to address the goodness of fit for each case and determine whether some models are preferred over others. As our main indicator of fit quality, we use the results of χ^2 test conducted by CIGALE. When conducting a fit based only on photometry, the calculation procedure goes as follows (Boquien et al. 2019):

$$\chi^2_{red} = \frac{1}{\sqrt{N-1}}\left[\sum_i\left(\frac{f_i - \alpha\times m_i}{\sigma_i}\right)^2\right] \quad (4)$$

where f and m are observed and modeled properties, and σ are associated errors. N refers to the number

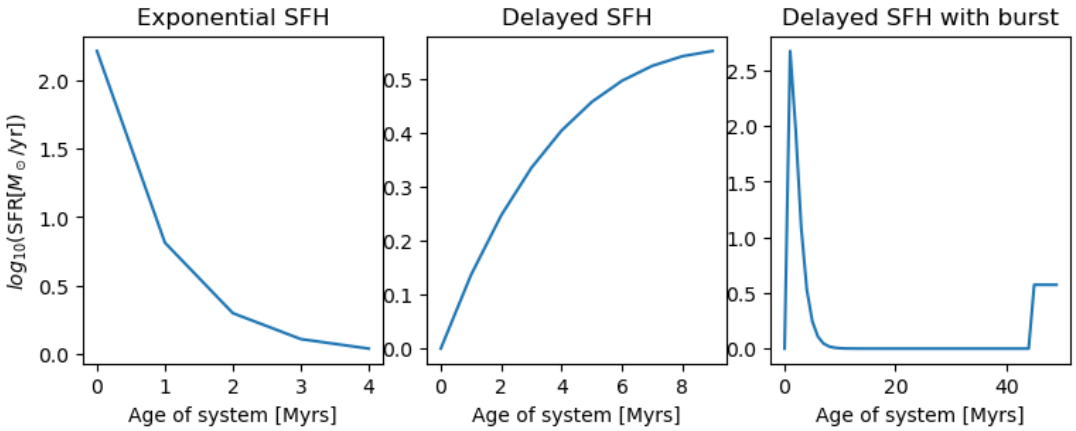

Figure 1: A visualisation of the three main SFH types considered in this work (ID 3638). Each subplot shows SFR as a function of age of the galaxy. Delayed SFH with optional burst is not displayed since in that case one of the other delayed cases will be chosen.

of filters used in the fit, thus the $\sqrt{N-1}$ reduction is applied to obtain a reduced χ^2, while α is a constant required for SFH normalization. In presence of upper limits the calculation gets more technical, and we refer the reader to Boquien et al. (2019) for a more detailed discussion. We report χ^2_{red} values ranging from 0.2 to 16, with a peak around 3 for all cases. Considering that the input was chosen based on prior knowledge about LAEs and parameter space is not overly restrictive, we inspect individual spectra and by observation conclude that high χ^2 values for certain objects are caused by small error bars in photometry combined with occasional outliers in certain filters, and are not necessarily indicative of a poor fit.

Choosing delayed SFH with no burst as our reference distribution, we compare our χ^2 values on a galaxy by galaxy basis in Figure 2. We highlight two highly significant properties of these plots: first, linear regressions of the scattered data all have slopes ≈ 1, meaning none of the star formation history models is systematically more favored than others and, on average, they are all alike. Moreover, the lack of significant scatter among the trend line shows that the χ^2 values are also comparable on an object by object basis. Therefore, there is not a clear answer as to which SFH model is more representative of our LAEs based on the goodness of fit alone. These observations are fundamental to our conclusions as they suggest that the variations in physical parameters we might discover for different star formation histories are all equally probable, and, due to this similarity in χ^2 distributions, the derived parameters should be interpreted with due caution.

The lack of a significant spread aroung the trend line corroborates our earlier point concerning poor-fitting galaxies: a high χ^2 is an effect of photometry and is not necessarily indicative of a poorly fitted SED. Nevertheless, two attempts have been made to improve the quality of the fit. First, through a visual inspection of spectra with high χ^2, several objects were identified having a problematic photometry in the F098M filter for HST WFC3_IR. Hence, we decided to re-run our SED analysis excluding this filter. As a result, 6 galaxies (3%) have a noticeably improved χ^2_{red}, with the difference going as high as 4 units. Fortunately, these outliers did not alter the shape of the fitted spectral model; we show a sample spectrum with improved χ^2 in Figure 3. By extension, our obtained physical parameters remained exactly the same regardless of F098M inclusion. In light of that, in subsequent chapters we will continue to work with a full set of filters for the sake of convenience.

Subsequently, there is an argument to be made against our assumption of E(B-V) of the stellar continuum being equal to the one of nebular lines. A number of studies (e.g. Calzetti et al. 1994, 2000; Buat et al. 2007) have shown that $E(B-V)_{neb}$ should be increased with respect to $E(B-V)_{cont}$. The principle argument behind selective dust extinction is that the nebular lines are located in starburst regions and are thus more prone to attenuation, while colder stars constituting the optical continuum have already drifted away from their parent cloud. We performed a fit setting $E(B-V)_* = 0.4\ E(B-V)_{neb}$, with the factor hailing from a recent derivation by Navarro-Carrera (2024, in prep). With this method, we find a decrease in χ^2_{red} of about 5%, but do not deem it significant enough to alter the fitting procedure.

In summary, our χ^2 analysis does not reveal a statistically significant preference for either SFH type based on the goodness of fit alone. Despite observing some relatively high χ^2 values, we find that these generally

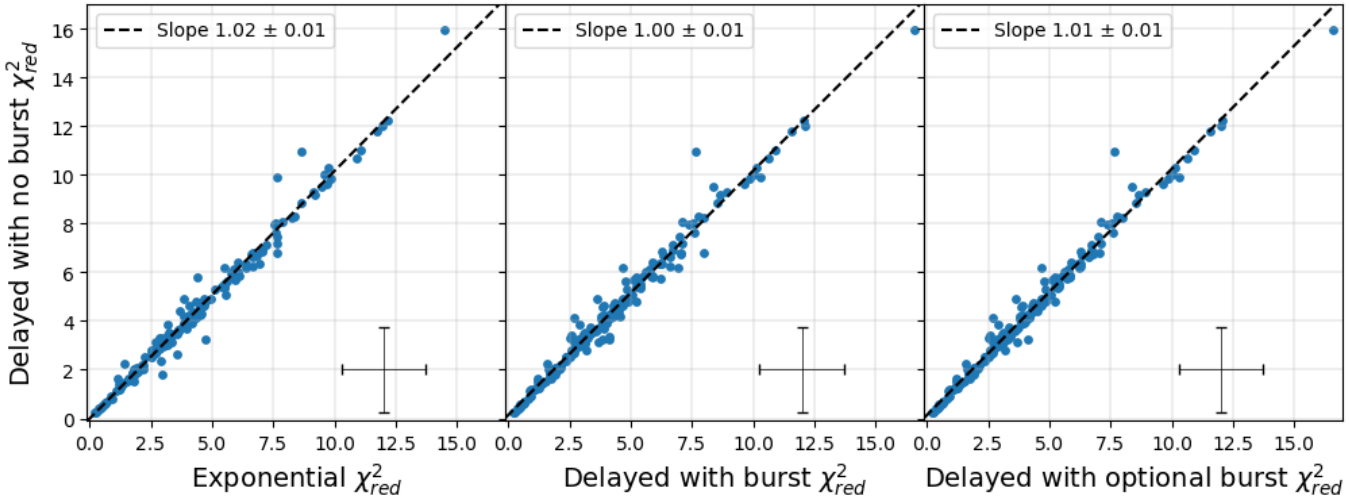

Figure 2: Comparison of reduced χ^2 for our objects among various star formation histories. The black dashed line shows the best linear fit of our data, with the slope and associated uncertainty indicated in the legend. Black error bars in the lower right corner represent the median errors of corresponding distributions.

happen due to small error bars in photometry rather than a flaw in the fitting process. Due to an inarguable similarity of χ^2 distributions shown in Figure 2, both on average as well as on a point-by-point basis, we highlight that there is no preference for either SFH parametrisation, and no results obtained from any model can be considered conclusive as a standalone.

3.3. *Derived SED properties*

3.3.1. *Impact of a recent burst among the delayed models*

We will start our discussion on the effect of a burst in star formation by first examining the case without the burst, for reference. We separate our LAEs in two age groups with the threshold of 100 Myrs, motivated by an approximate lifespan of O and B stars producing rest-frame UV emission (Soderblom et al. 2014). However, it is important to note that throughout our research the age under consideration is mass-weighted, and is therefore representative of the age of stars constituting the most mass within the galaxy, and does not directly indicate the time of the beginning of star formation. Thus, from now on we will refer to LAEs with a mass-weighted age less (more) than 100 Myrs as young (resp. old).

For our reference SFH, we recover a strong presence of young objects constituting 81% of our sample. This may indicate a separation between young and old populations, which is why we show the relative distribution of some of their physical parameters in Figure 4.

An important implication of this graph ought to be addressed: we find a strong bimodality in stellar mass distribution between the age groups, indicating that young LAEs are less massive objects, but with star formation rate still comparable to older LAEs. This separation carries itself over to sSFR, the implications of which are discussed in more depth in Section 3.4.

The separation between two age groups is in line with a number of previous studies. Arrabal Haro et al. (2020) studied a set of 404 high-z Ly-α emitters and recovered a 67% fraction of young LAEs with lower mass. A similar result was obtained by Ning et al. (2024), albeit with a highly constricted sample of 14 LAEs and only 4 fitted photometric data points. Finally, Iani (2024) performed SED fitting on the same set of 182 LAEs and derived almost identical results to us, with 72% of galaxies being younger than 100 Myrs and stellar mass in the 10^{7-8} $M_\odot$ range.

In order to quantify this separation, we perform a Kolmogorov-Smirnov test (henceforth KS test) on the physical parameter distributions between the two age groups. Following Iani (2024), we create 200 perturbations within each data set about its corresponding 1σ interval, and perform a KS test on each possible permutation of the perturbed versions of our data. As a final p-value we adopt the mode of the 40 000 p-values created from cross-matching the distributions, and report the result in the first row of Table 1.

Adopting a null hypothesis that the samples come from the same distribution, we set $p = 0.05$ as a minimum value for statistical significance. Judging from the results we obtained, there is indeed a very clear indication that stellar mass and sSFR are segregated by age, while UV continuum slope, SFR and, to a lesser extent, dust attenuation are comparable.

Having understood the general behaviour of the LAEs in our sample, we will proceed to observe possible discrepancies when a constant burst is added. We have

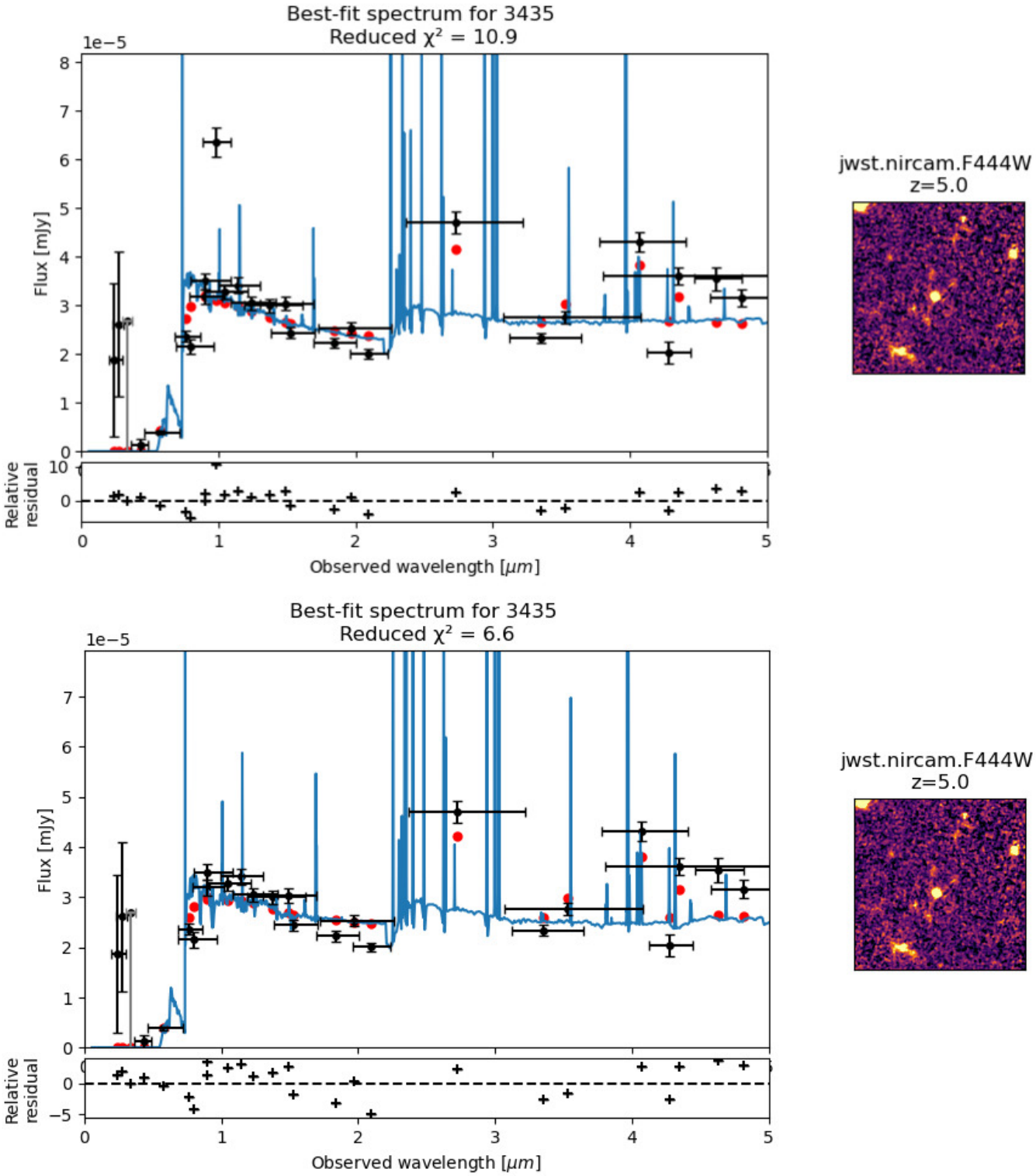

Figure 3: Example of a misdetection in the F098M filter as seen in one of the objects' spectrum (ID 3435). Both spectra show the photometry (black) with best flux estimates from CIGALE (red) along the spectrum, with the bottom image representing a run without F098M (outlier at $\lambda_{obs} \approx 1\mu m$ in the top spectrum). Upper limits are shown in gray. We complement the spectrum by showing a 5" × 5" cutout of the galaxy in NIRCam/F444W (Rieke et al. 2023), as well as relative residuals in the bottom panels computed as $\frac{\text{flux}-\text{fitted flux}}{\text{error}}$.

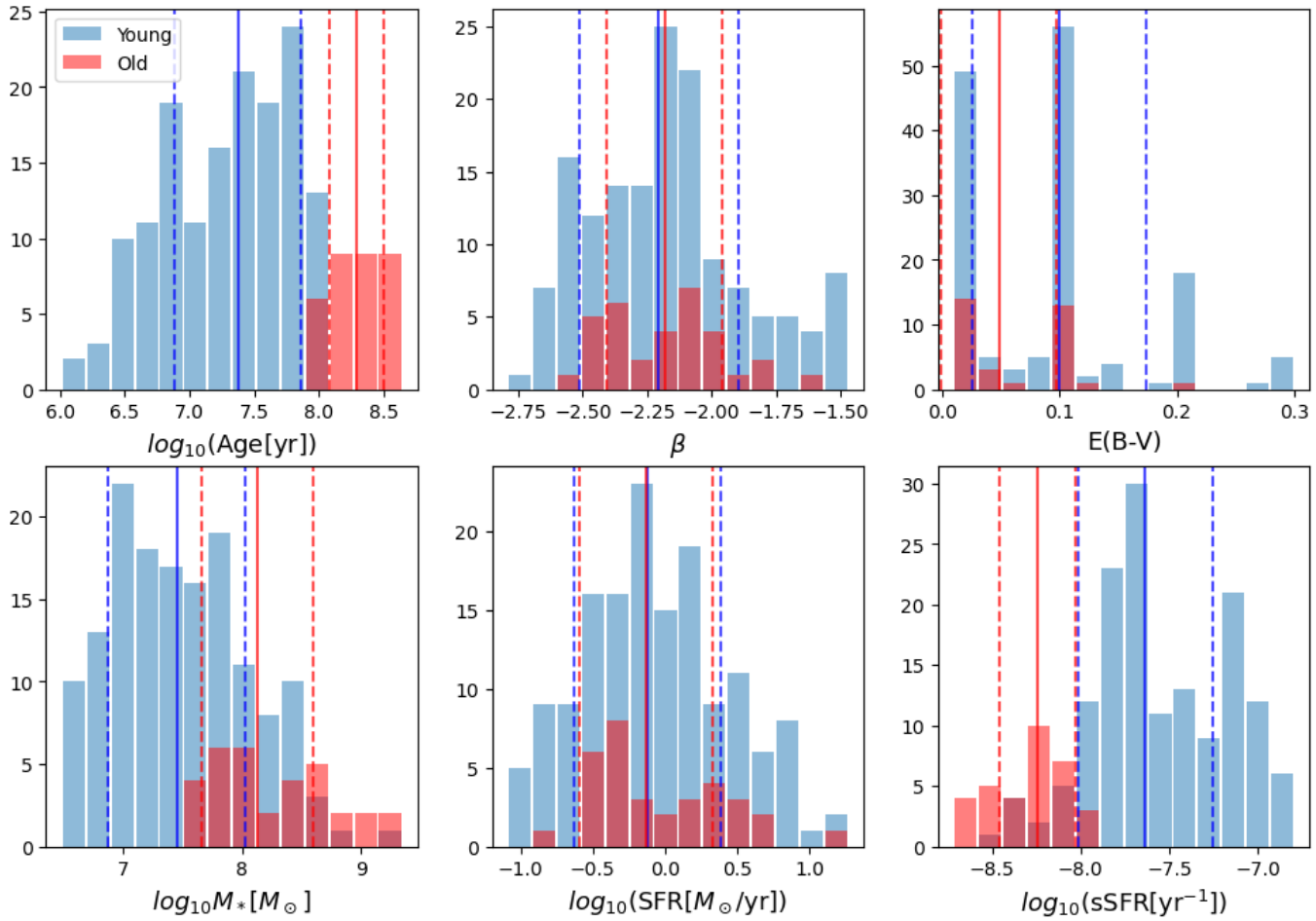

Figure 4: Distribution of physical parameters obtained from SED fitting using delayed SFH with no burst (note that the demonstrated SFR are not obtained from the fit, see Section 3.1.2). Young LAEs ($\leq$ 100 Myrs) are colored in blue, while old ($>$ 100 Myrs) are in red. The vertical solid lines show the median values within corresponding age groups, and the dashed lines indicate a 1σ interval around the median. The visualization style was adapted from Figure 8 in Iani (2024).

	β	E(B-V)	M_*	SFR	sSFR
No Burst	$0.53^{+0.21}_{-0.37}$	$0.16^{+0.13}_{-0.14}$	1e-5	$0.49^{+0.34}_{-0.18}$	5e-15
Burst	$0.43^{+0.22}_{-0.27}$	$0.07^{+0.14}_{-0.05}$	5e-3	$0.52^{+0.27}_{-0.31}$	1e-8
Optional Burst	$0.32^{+0.24}_{-0.18}$	$0.06^{+0.14}_{-0.05}$	2e-3	$0.33^{+0.47}_{-0.15}$	9e-8

Table 1: Results of the KS test for physical parameters of young and old LAEs assuming a delayed SFH. The values are p-values with their respective 68% confidence intervals. For p-values < 0.05 errors are not reported since their magnitude is insignificant.

fitted two cases: one mandates a burst, while the other lets CIGALE choose whether a burst should be fitted or not. This framework was chosen as it allows us to both study the implications of a bursty SFH, as well as note whether such SFH is preferred over one with a single component.

We present the distribution of the main physical parameters obtained from both cases in Figure 5. At first glance, the distributions look alike. Such a similarity would only occur if the burst is preferred for the majority of LAEs, and a simple check reveals that 154 objects (85%) choose to fit a burst when this possibility is allowed. We believe this may be correlated with the allowed ranges of fitted age: a large portion of most recent star formation responsible for Ly-α emission will have to have happened recently, and since the burst takes up the last 15 Myrs we would expect it to be chosen in the majority of cases. Given these insights, we proceed to examine the differences among key physical parameters, namely the SFR, stellar mass and mass-weighted age.

First, we point out a very distinct similarity between both bursty cases. This was anticipated, since such a large percentage of our LAEs choose to have a burst when presented the opportunity. Thus, in our further analysis we will stop considering the SFH with a mandatory burst as a standalone, motivated by the extent of its agreement with the optional burst case. All conclusions and implications derived from the behaviour of delayed SFH with optional burst will be indicative of the one with mandatory burst as well.

As to the individual physical parameters, we do not observe a meaningful change in star formation rates since we only consider our empirical approximation. The only reason the SFR distributions drift from fit to fit is the E(B-V) value used in the dust correction of absolute UV magnitude, and since the scatter is mild and unsystematic we attribute it to a binning in the fitted dust attenuation values.

On the other hand, the stellar mass distributions require a more thorough investigation. In general, all three cases seem to agree well with each other, which one would expect since stellar mass is mostly determined through the level of continuum and all fits should reproduce the same photometric points. However, we note a systematic scatter among young LAEs, with a tendency towards higher stellar mass when the burst is present.

The interpretation of this behaviour is tightly linked to the relative distribution of ages. Both with and without the burst, the mass-weighted ages among older galaxies are in good agreement. On the contrary, for younger galaxies the trend deviates from linearity and upturns at ≈ 15 Myrs. This occurs due to our fitting assumptions: by adding a burst, we involuntarily prevent the main stellar population from being younger since burst is not allowed to be older than the underlying component. As a result, the youngest galaxies (≤ 15 Myrs) can only be modeled with a burst, and therefore would require a much older underlying population to reproduce the rest of the spectrum. In that case, the old component tends to fold very quickly in order to avoid adding even more blue light to the fitted SED, with as many as 76 (86%) of those objects fitting an e-folding time of main component ≤ 10 Myrs. This timescale is very short compared to the old component's age (median ≈ 180 Myrs), which is indicative of very weak star formation activity superseded by passive behaviour until the recent burst. As a result, most of these objects are still considered young under our definition as weighing by mass smooths out the bimodality of their SFH, and the total fraction of young galaxies does not decrease.

Coming back to the stellar mass variation, it is now clear that fitting an older component would not preserve the stellar mass of the galaxy, resulting in a slight trend towards higher masses for young LAEs. Since mass is well-known to be a robust parameter in SED fitting due to lack of degeneracies (Pacifici et al. 2023), its stark deviation requires a check of fit quality for the corresponding objects.

For this reason, we focus on LAEs with a stellar mass increase of ≥ 0.2 dex (27 objects), and find a median decrease in χ^2_{red} of $0.27^{+0.71}_{-0.33}$ units when the burst is added.[1] We then inspect the fitted spectra and identify two main reasons why adding an underlying population has such a weak impact on fit quality. For some objects, the data at longer wavelenghts is associated with very large error bars and/or upper limits, likely due to young galaxies being faint in red bands thereby increasing the uncertainty of the measurement. A slight rise in the continuum therefore still accommodates JWST photometry, and no change in χ^2 occurs. On the other hand, in cases where the errors are small enough to detect a mass change, the objects are redshifted enough to reduce the number of photometric data points spanning long wavelengths. Thus, the extrapolation of the SED after the last photometric data point can afford to change continuum levels without affecting the fit, raising the stellar mass with no χ^2 increase.

We can see this characteristic reflected in relative distributions of young and old LAEs when the burst is present. Referring back to Table 1, we highlight an

[1] In this case, the lower bound results in a negative decrease (i.e. an increase) in χ^2_{red} with a burst present.

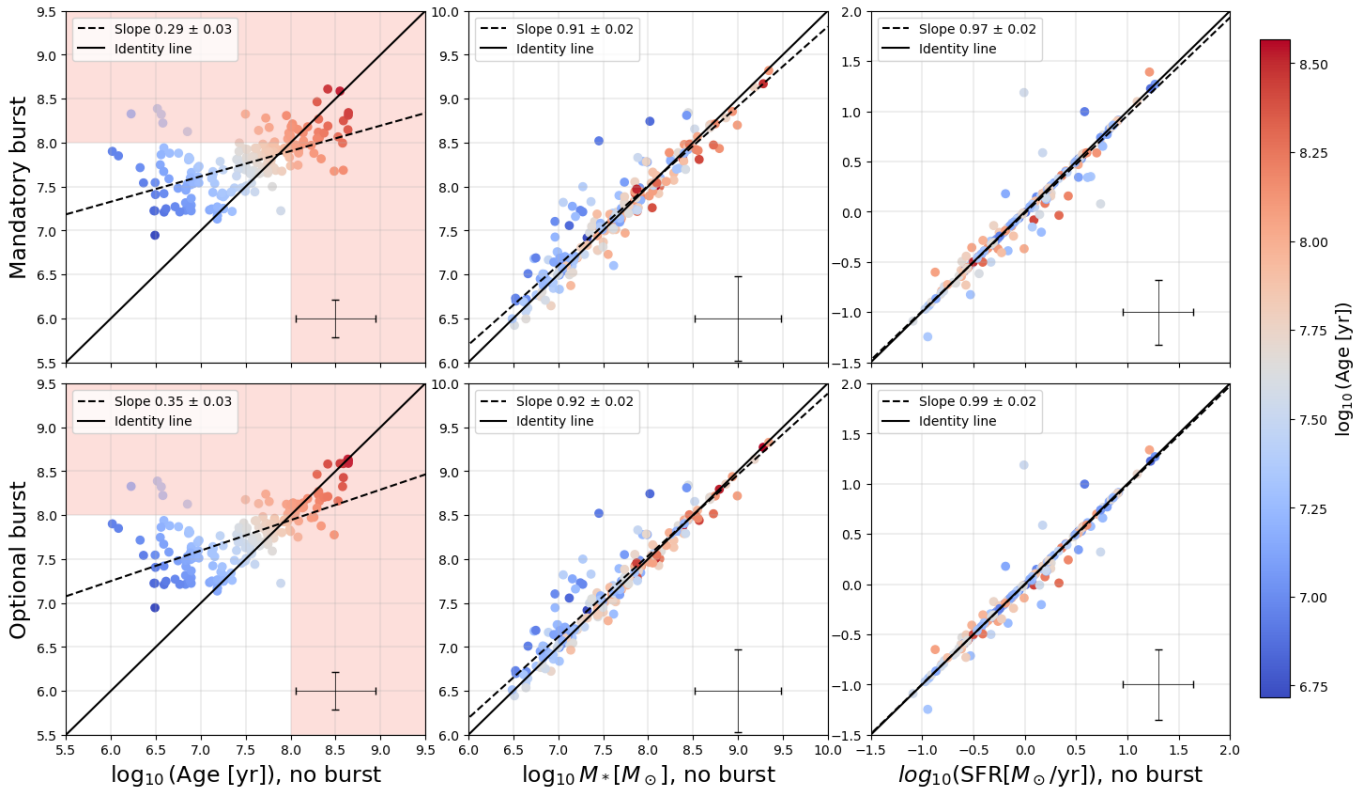

Figure 5: Comparison of the physical parameters obtained for delayed SFH with no burst (horizontal axis on all plots) against delayed SFH with mandatory burst (first row) and with an optional burst (second row). Each column corresponds to one parameter considered: Age (mass-weighted), Stellar mass, and SFR respectively. We color code the LAEs based on their average age between the two SFH models, and complement the plots with an identity line (black, solid) and best linear fit (black, dashed) with the corresponding error. The shaded region on the age vs age plots is meant to represent the space occupied by old LAEs ($>$ 100 Myrs), while the errors in the corner refer to the median errors.

increase of p-value for stellar mass by 3 magnitudes and sSFR by 7 magnitudes. Certainly, our KS test results can vary due to the way distributions are randomly perturbed, but we do not expect to see a difference that large from the method alone. Therefore, we conclude that the M_* and sSFR distributions of young and old LAEs become much more similar when a burst is present, and for more details we refer the reader to Section 3.4

3.3.2. *Exponential SFH*

Exponentially declining star formation history is one of the most frequently adopted SFH models for SED fitting. However, several works showed it to be inaccurate in comparison to other models, particularly when applied to high-z star-forming galaxies (see Maraston et al. 2010; Reddy et al. 2012). Physical parameter estimation using exponential SFH was also shown to be off by Simha et al. (2014); Pacifici et al. (2015), mainly because this type of SFH assumes that the galaxy's star formation is at its all-time minimum which might not be an accurate premise. As was pointed out by Maraston et al. (2010), assuming an exponentially rising SFH would produce better results for objects at high z as it better reflects the behaviour of young galaxies with intense star formation.

For our fit using delayed SFH with no burst, we have mainly corroborated these results. Since the e-folding time of the main stellar component also specifies the time of the peak, CIGALE is allowed to fit galaxies with $\tau >$ age, effectively forcing them to have an ever-increasing SFR. As a consequence, we observed 60 galaxies (33%) to have an e-folding time larger than the age of main stellar population, and 50 more galaxies have their τ_{main} within 0.5 dex of their physical age. That brings the total number of LAEs for which the SFH is mostly increasing to 60%. These galaxies then dramatically change their SFH when burst is added, with no increase in χ^2_{red} (see Figure 1 for a clear example). Thus, by comparing the tau model to a delayed one, we will be able to assess how much discrepancy there is

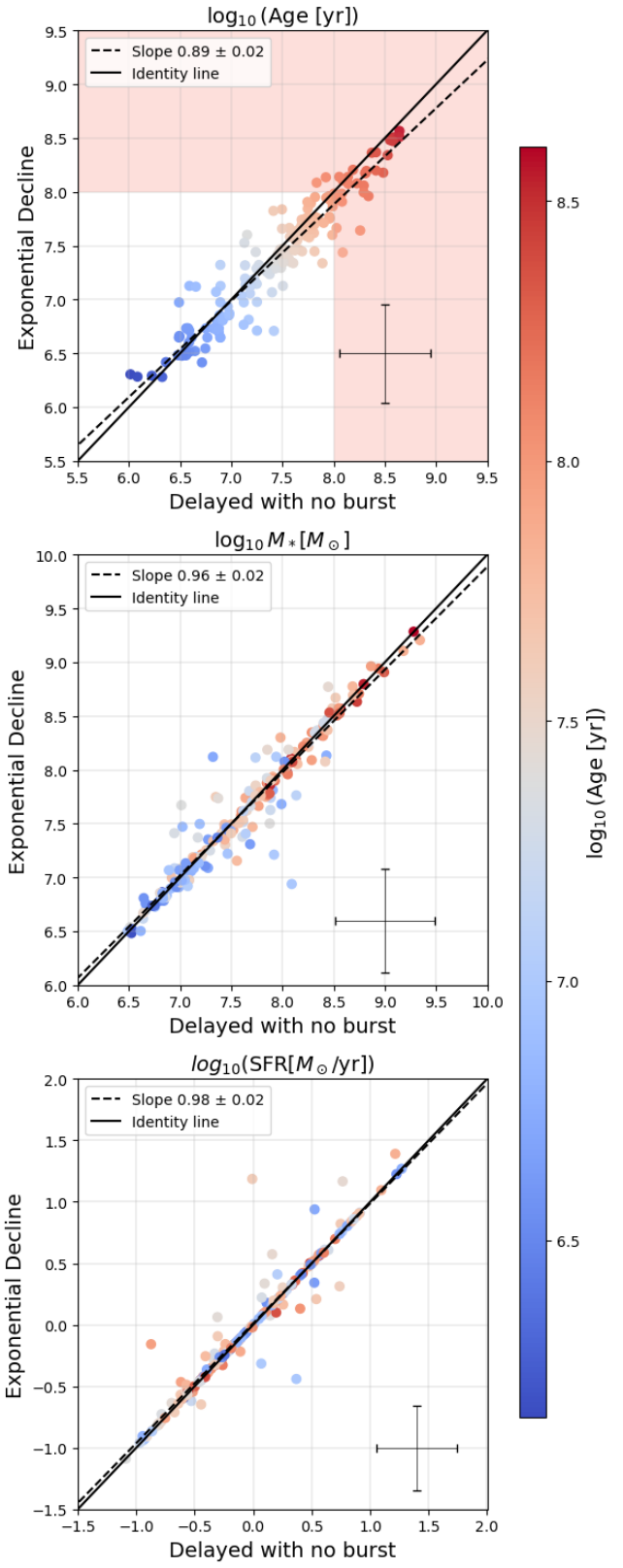

Figure 6: Comparison of the physical parameters obtained for exponential SFH against delayed SFH with no burst. We color code the LAEs based on their average age between the two SFH models, and complement the plots with an identity line (black, solid) and best linear fit (black, dashed) with the corresponding error. The shaded region on Age vs Age plots is meant to represent the space occupied by old LAEs (> 100 Myrs), while the errors in the corner refer to the median errors.

in parameter estimation for our data set, depending on whether the SFH is (mostly) rising or declining.

We present the relative distributions of age, stellar mass and SFR for exponential SFH in Figure 6. Despite the fact that an exponentially declining SFH is not the most correct parametrisation for a LAE, the best-fit parameters are stable enough to not impact the final result significantly: SFRs and masses are in very good agreement with each other, and the scatter is minimal and unsystematic. The ages for both models are very similar as well, albeit with a thicker spread and a slight tendency for younger ages for the exponential case. In that way, the discussion from Section 3.3.1 on physical properties of LAEs assuming a delayed SFH with no burst can be broadly extrapolated towards an exponential SFH.

Something similar was shown by Carnall et al. (2019), who considered the effects of assuming 4 different SFH types (among which exponentially declining and delayed) on the fitting outcome, and found no significant inherent biases for each case. However, it is necessary to point out that their sample was redshifted. Overall, considering a lack of χ^2 difference between the two models (Section 3.2), we conclude that the exponential SFH is as representative of our LAEs as the other star formation histories, both in terms of fit quality as well as physical parameter estimation.

3.4. *SFR-M_* and sSFR-M_* planes*

The relation between stellar mass and star formation rate is widely used to quantify various stages of galaxy evolution. Most galaxies lie along the main sequence (MS), which predicts a higher star formation for more massive galaxies (Noeske et al. 2007). This relation is often modelled as a power law (Speagle et al. 2014; Rinaldi et al. 2022), with the existence of a clear trend across a wide range of stellar masses implying that those galaxies share similar evolutionary paths.

However, it was later shown that some galaxies place themselves significantly above the MS, particularly at high redshift. The emergence of these starbursts (SBs) remains uncertain, but their relatively high fraction (16% at $2 < z < 3$, Bisigello et al. 2018) highlights their importance in the cosmic star formation history. In this subsection, we examine the placement of our sample of Ly-α emitters in both SFR-M_* and sSFR-M_* planes for different star formation histories, following Caputi et al. (2017, 2021) in defining SBs as galaxies with specific star formation rate (sSFR) ≥ -7.60. We present our results for a traditional τ-model, delayed with no burst, and delayed with an optional burst in Figure 7.

Assuming exponentially decaying star formation, we recover the traditional bimodality between young and

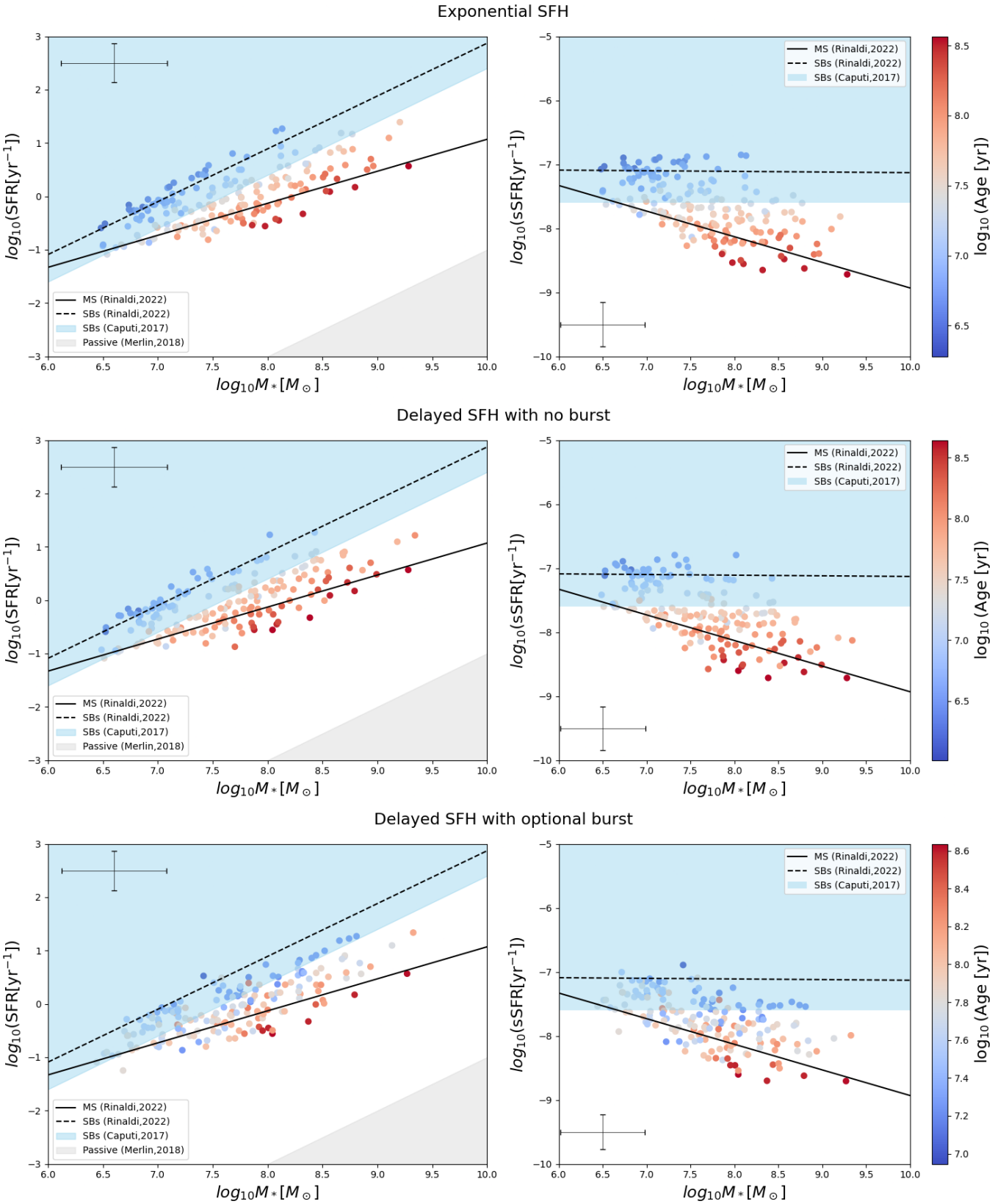

Figure 7: SFR-M_* and sSFR-M_* planes as a function of SFH, where each row is indicative of a different SFH model (exponential, delayed and delayed with an optional burst resp.) The blue shaded region represents the area occupied by starburst galaxies (SBs) (sSFR $\geq 10^{-7.6}$ yr^{-1}, Caputi et al. 2017, 2021), while the grey region is indicative of passive galaxies as shown by Merlin et al. (2018), with sSFR $\leq 10^{-11}$ yr^{-1}. We color code our LAEs based on their estimated age for each given SFH, and complement each plot with main sequence (MS) and SB trendlines (solid, dashed) at $z \approx 4$ obtained by Rinaldi et al. (2022). We also report the median errors of the distributions in the corner of each plot. Presentation style was inspired by Figure 7 from Iani (2024).

old LAE populations, with the former following an estimated starburst sequence from Rinaldi et al. (2022) while the latter keep to the MS trend. The same result for this SFH was obtained before, and the distinct splitting by age is usually interpreted as a sign of all LAEs being similar galaxies at a different evolutionary stage (Rinaldi et al. 2022, 2024; Iani 2024).

Switching to a delayed model does not seem to change much in this regard. The only change we observe in the relative distribution of the two age populations is a more prominent gap in between: while before the scatter had a roughly constant density, now we observe more distinction between the groups with an empty space in between. Referring back to Chapter 3.3.2, we recall the only major distinction between those fits, mainly that we find a lot of young galaxies with age $\leq \tau_{main}$, or an increasing SFH. This effect might cause more bracketing between the age groups, since in a delayed SFH the star formation rate goes through a rising phase, a peak and a decline, leading to a more significant separation between actively star forming galaxies and more passive ones.

The situation appears to be different when an optional burst is added. As was pointed our in Chapter 3.3.1, although we do not observe a difference in SFR, we do get a stellar mass increase among the young LAEs, meaning younger galaxies drift horizontally from the SBs region towards the main sequence. This behaviour results in the entire distribution resembling one population with a scatter rather than two segregated ones, mainly because young LAEs fill the gap between the age groups.

On the other hand, the galaxies that do stick to the SBs trend are ones with the smallest mass and largest burst fraction fitted, with a mean value of 0.2 but going as high as 0.99. We would not normally expect a recent burst to dominate the stellar mass of a galaxy, since it is usually determined by the underlying population (Schawinski et al. 2007). In other words, even a strong burst would constitute a small stellar mass fraction when compared to an existing old population. Therefore, high burst fraction values indicate the lack of a prolific underlying stellar component, with the majority of stars originating from the recent burst. This effect happens due to the numerical restriction we had to impose on the minimal age of the main stellar component: it cannot be younger than 15 Myrs since younger ages are used to accommodate the burst. As a result, very young (≤ 15 Myrs) star-forming galaxies are best represented by the burst, and have very high burst fractions. Their underlying population is usually extremely old (up to 1 Gyr) with a very short e-folding time, minimizing the effect of the old component on the SED.

This can also be seen when considering the ages of these objects. Without a burst, SBs with the lowest mass are the youngest galaxies of the sample (≈ 3 Myrs or $10^{6.5}$ yrs, see the top and middle row in Figure 7). When the burst is added, the same objects return a considerably higher age of ≈ 60 Myrs or $10^{7.8}$ yrs. Since our definition of age is mass-weighted, the burst contributes a low age value with a higher weight, while the small underlying population adds a very high value with a low weight, resulting in an overall elevated age estimation when compared to a single-component SFH. For that reason, the reader has to be careful when interpreting the bottom panel of Figure 7: the color coding might be misleading when comparing it to the top and middle ones. Since we did not find any LAEs younger than 10 Myrs when a burst is present, the colors were shifted accordingly, with the same color now representing slightly older galaxies.

All in all, this phenomenon explains why these low-mass LAEs still follow the SB trendline, as they mostly consist of the stars formed in the recent burst. On a side note, since old galaxies were not shown to increase their stellar mass, we find them still conforming to the MS slope.

When considering the LAEs that deviate from the starburst line and drift towards the main sequence, an argument could be made that starburst and main sequence lines change with redshift since cosmic star formation rate is variable with time (Lehnert et al. 2015). In that way, fitting a sample of 182 LAEs with $z \approx 3-7$ to a line derived for $z = 4$ is technically an approximation. However, the deviations in slope and intercept are slight and stay mostly within each other's error range (Table 3 in Rinaldi et al. 2022), so we would not observe a significant difference when adopting either line in our redshift range. Besides, the same trend lines fit the data very well for both SFH models without a burst, thus we can have relative confidence when presuming that the issue lies in the data and not its representation.

A seemingly similar trend was observed in ILLUSTRIS, a hydrodynamical simulation modelling galaxy formation and evolution up to $z = 4$ (Springel et al. 2018). As a criterion for deviation from starbursts, a percentage of galaxies above the MS relation was used, and the estimated fraction of SBs was $< 15\%$ (see Figure 4 from Sparre et al. 2015). However, when we compute the fraction of galaxies that populate the sSFR> -7.6 yr^{-1} region, we observe little difference between the three models: 43% for exponential SFH, 38% for delayed without a burst and 36% when the burst is added. Rinaldi et al. (2022) reported a similar fraction of 52%, performing a τ-model fit on a similar sample

in LePHARE. In that way, our results are at odds with ones predicted by ILLUSTRIS.

As was also argued by Rinaldi et al. (2022), the mass range studied by ILLUSTRIS is $10^{9-11.5}$ $M_{\odot}$, which is significantly higher than that of the LAEs in our sample. Besides, its resolution of 1 kpc could impact the simulated results, since it might not allow for accurate modelling of events such as mergers or instabilities, which are known to trigger intense bursts of star formation.

All in all, we emphasize that even though some LAEs were shown to deviate from expected trends, the overall fraction of starburts in our LAE sample does not change as a function of SFH and we observe a similar number of objects with sSFR $\geq 10^{-7.6}$ yr^{-1} for all cases. A slight drift of young LAEs towards the MS might indicate is that Ly-α emitters are not necessarily similar galaxies in different evolutionary phases, but older objects going through rejuvenation instead. However, we must keep in mind that this conclusion is only based on an increase of stellar mass among young LAEs, and, as was also discussed in Chapter 3.3.1, it is correlated with a loose constraint on rest-frame optical and NIR parts of the spectrum. In light of this and a lack of significant change in χ^2_{red} compared to other SFH models (Section 3.2), we cannot exclude that this occurs only due to numerical reasons.

4. DISCUSSION ON THE IMPORTANCE OF VARIOUS DATA SETS

Throughout our research, we have built upon a robust initial base of photometric measurements comprising 27 bands. The photometry included a roughly equal distribution of HST and JWST bands, featuring 19 wide bands complemented by 8 medium bands. Such comprehensive dataset allowed us to constrict the spectra and determine physical attributes of 182 LAEs. In this chapter, we address the necessity of such holistic photometry for accurate SED fitting by sequentially excluding certain types of data and evaluating the outcome. First, we will exclude the JWST data and perform SED fitting based on only HST bands, followed a second analysis without medium bands.

4.1. *JWST photometry*

Due to the wavelength range covered by HST, observations of highly redshifted objects is challenging (Tilvi et al. 2016). While HST surveys could be useful for the detection of Ly-α emitting galaxies through rest frame UV emission, they are not sufficient to distinguish the shape of the spectrum beyond the Balmer break ($0.36\mu m$). For that reason, JWST coverage is crucial for a comprehensive spectral analysis (for a more descriptive example of wavelength ranges spanned by each instrument, we refer the reader to Figure 9 from Iani (2024) and the discussion surrounding it). In an attempt to quantify the discrepancies, we discard JWST photometry and perform a fit based only on the data available from HST, and compare the outcome. This exercise will be performed for our reference case of delayed SFH without a burst.

The distribution of selected physical parameters can be seen in Figure 8. Inspecting the data, there is only one discussion to be had, and that is on parameter degeneracies. A degeneracy occurs when more than one feature can reproduce the photometry equally well, causing the software to "guess" the appropriate one. A priori, a degeneracy is only possible when photometry is not constrained enough, which causes the prior to be the same as the likelihood as there is no weighing to be made (da Cunha et al. 2008, 2015). This is the exact position we have put ourselves into, as HST lacks rest-frame optical and IR coverage of our objects, making it difficult to adequately constrain features of the spectrum at those wavelengths.

Some well-known degeneracies involve redshift, dust attenuation, SFR, age and metallicity, since all of those parameters cause reddening in a similar way (Dunlop et al. 2007; Pacifici et al. 2023). We have constrained the redshift to its spectroscopic estimate, calculated SFH empirically, and do not expect large variations in metallicity since LAEs are known to be metal-poor systems (Ouchi et al. 2020). Therefore, our attention is directed mostly towards age and E(B-V).

Observing the behaviour of data points, we note a distinct lack of young dusty objects in the E(B-V) panel (bottom right), with a tendency towards lower extinction. On top of that, although the overall fraction of young LAEs does not change, we observe a rise in the median age by almost 0.3 dex. We believe these trends are related, and discarding JWST data causes CIGALE to mistake young galaxies with higher E(B-V) for slightly older dust-poor objects. Lower dust attenuation is then carried through dust correction into our SFR estimates, which decrease since lower dust content would imply less burstiness. As to the stellar masses, since they have no known degeneracy we conclude that due to lack of data, CIGALE cannot estimate the continuum level accurately, resulting in a large scatter about the Mass-Mass identity line (up to 1 dex).

A similar result was obtained by Haskell et al. (2023), who split their photometry into a stellar part ($0.4\mu m \leq \lambda \leq 2.2\mu m$) and far infrared part ($100\mu m \leq \lambda \leq 500\mu m$), performing an SED fit for each case and com-

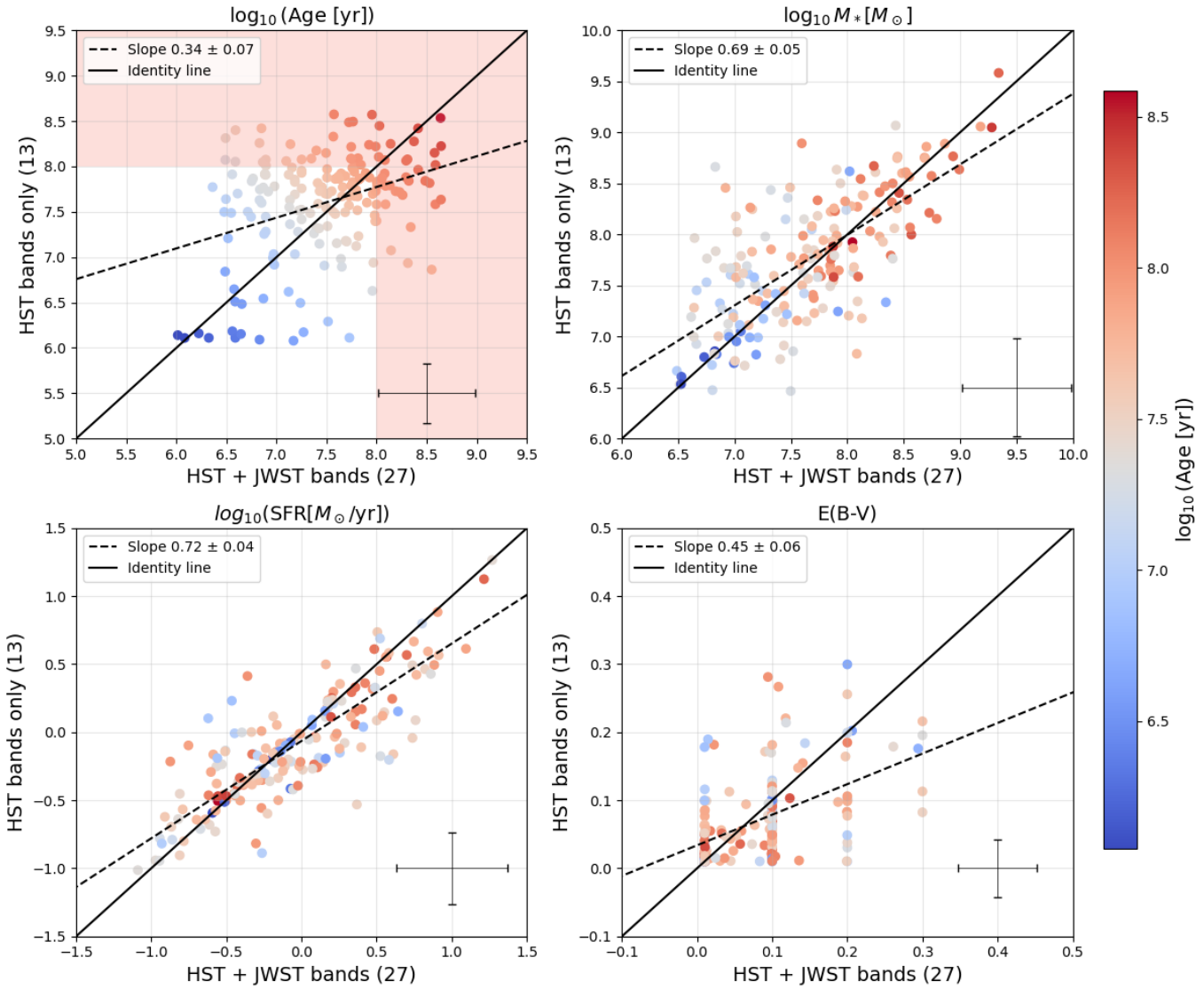

Figure 8: Physical parameters compared between a fit with all photometry and with HST bands only. We color code the LAEs based on their average age between the two SFH models, and complement the plots with an identity line (black, solid) and best linear fit (black, dashed) with the corresponding error. The shaded region on Age vs Age plots is meant to represent the space occupied by old LAEs (> 100 Myrs), while the errors in the corner refer to the median errors.

paring the quality of outputs. Even though the gap between those wavelengths is much larger than between our HST and JWST median coverage, the results of this experiment are still indicative of a trend we could expect. Naturally, using either one set of filters by themselves resulted in a much worse constrained estimate then using composite photometry. Reintroducing JWST filters would therefore constrain a significantly larger portion of the spectrum, allowing for a more precise likelihood estimation and breaking though the degeneracy stalemate.

4.2. *Medium-band photometry*

Compared to wide bands, mid-band filters span a narrower wavelength range and compensate for it with an increased resolution. This allows mid-band surveys to provide more detail about particular parts of the spectrum by probing them in greater depth. In practice, these features make mid-band photometry a powerful tool while studying emission lines.

For instance, while searching for extreme emission-line galaxies, Withers et al. (2023) highlights the advantages of medium-band photometry over wide bands. A narrower sampling of mid-band filters allows for more re-

fined spectra with less source contamination, ultimately leading to the detection of 118 new objects through their H_α emission which otherwise would have been missed. Moreover, medium-bandwidth filters were shown to double the precision of spectroscopic redshift estimation, as was shown by Whitaker et al. (2011).

With these advantages in mind, it is clear how such filters are particularly useful for detecting and studying galaxies with strong Ly-α emission. However, since the redshift values of our LAEs originate from a different study where all bands were used, we cannot quantify the mid-band contribution to the redshift estimate. Thus, we will focus on performing an SED fit using only wide-band detections (19 filters out of 27) at fixed redshift and discuss the implications. Again, for this test we adopt a delayed τ model with no burst.

Our results indicate minimal deviations among stellar mass and SFR, with both datasets lying along the identity line with a scatter within 0.3 dex when compared directly. However, we observe CIGALE slightly diminishing the effects of dust for a number of objects, even though the general trends with and without mid-band photometry are very similar (0.92 correlation). The little discrepancy we discover could either be caused by binning in the E(B-V) values, or by an underestimation of star forming activity since emission lines are not resolved anymore. The age distribution is fairly well-modelled for younger LAEs, but becomes more scattered for older galaxies, mostly with a tendency for slightly lower ages. As discussed by da Cunha et al. (2015), age estimates coming from broad-band photometry alone can be inaccurate due to age-dust degeneracy and the fact that young stars are much more luminous, outshining older stars and making them less visible when the filter is shallow. Since we have extensive JWST coverage, dust effects are well accounted for and degeneracies are unlikely. Therefore, we conclude that due to the luminosity of young stars some members of the underlying population might not be resolved, thereby causing a slight underestimation of age.

Recent works by Papovich et al. (2023); Ning et al. (2024) could be seen as examples of limitations caused by minimal photometry. For the fitting procedure, they relied on detections in only 4-5 wide bands, resulting in poorly constrained physical properties. Thus, a comprehensive dataset, spanning various wavelengths and including different bandwidths, is indispensable for accurate parameter estimation. This approach breaks through parameter degeneracies and treats objects of uneven brightness on an equal footing, which is a key point of this chapter.

5. CONCLUSIONS

In this work we have performed an SED fit on a set of 182 confirmed high-redshift Ly-α emitters. We considered two main SFH types, exponentially declining and delayed, and investigated the differences in their corresponding outputs. The delayed model was then complemented by an option to fit a continuous recent burst of star formation, allowing us to further explore the impact of star formation history on recovered physical properties of those LAEs. Our key findings are:

- Choosing delayed SFH with no burst as our reference distribution, we find a clear bimodality between the properties of young (< 100 Myrs) and old (≥ 100 Myrs) LAEs. Young galaxies constitute the majority of our sample (81%), have a lower stellar mass ($10^{7-8} M_\odot$) and higher dust attenuation (up to 0.3 mag). These results are in strong agreement with prior literature on properties of Ly-α emitters.

- We do not observe a significant difference between physical properties extracted from exponential and delayed models. Considering that most of our LAEs (60%) exhibit a rising SFH in the delayed model, we conclude that both declining and rising SFH models are equally representative of our sample.

- Allowing for a burst in the delayed SFH causes a deviation in parameters of young LAEs, mainly age and stellar mass. We find that very young galaxies become significantly older and resemble a rejuvenating galaxy rather than a recently formed one, which is likely a combination of SED preference and numerical restrictions imposed during the fitting procedure. This same phenomenon causes the mass of some young LAEs to increase by roughly 0.5 dex, since the photometry of those galaxies does not allow to constrain the stellar mass of the underlying component.

- Our χ^2 analysis shows similar results for all cases, indicating no preference for any of the star formation histories considered or burst presence. We therefore cannot conclude that one set of results is more likely than the other, and both exponentially declining and delayed SFH models, with or without burst components, can adequately describe the observed SEDs.

- On the SFR-M_* and sSFR-M_* planes, we retrieve variable results. When assuming any SFH without a burst, we observe the well-known bimodality in

the relative distribution of young and old LAEs, with the former following a starburst line while the latter go along the main-sequence (Rinaldi et al. 2022). When a burst is added, the separation becomes less evident and young LAEs are placed closer to the MS region, while the fraction of galaxies defined as starbursts (sSFR $\geq 10^{-7.6}$ yr^{-1}) is mostly maintained. We attribute this shift to an increase in stellar mass among younger objects, since the SFR was estimated empirically and thus remained largely unchanged. This might indicate that LAEs are older than previously thought and are experiencing rejuvenation, but we cannot exclude the possibility of it being a numerical artifact. In the future, we propose considering the % of galaxies within the starburst region as defined in Caputi et al. (2017, 2021), since we found it to be much more robust among the SFH types.

- Finally, we tested the performance of parts of our photometry when considered in isolation. Discarding JWST data, we discovered heavy age-dust degeneracy due to a limited coverage of HST bands. Even stellar mass, typically the most robust parameter, showed a large scatter of up to 1 dex since the rest frame optical/NIR is redshifted beyond HST coverage and the SED at those wavelengths was not constrained. Then, excluding medium-band observations leads to a problem of outshining, causing a general age underestimation since faint older populations become more difficult to resolve. Overall, these results underscore the necessity for an extensive photometry which spans various wavelengths and resolutions.

There are always steps to be considered in order to build upon these results, particularly when discussing star formation histories. Introducing a prior could guide the software towards the most suitable SFH, potentially creating a more physically reliable result. For that, one might consider applying BIC model selection which would prioritize models with less parameters (Schwarz 1978), or complementing the SED by spectroscopical data.

Besides, non-parametric SED fitting codes are becoming more prevalent (Leja et al. 2019, and references within), and their flexibility might allow to accommodate a much greater variety of SFH models. That might resolve the issue of biased properties estimation common in parametric software. But even then, one must always keep in mind the existence of code-specific biases, as no matter how advanced a code is there are always assumptions underneath. In that way, an objectively true result might not ever be attainable due to the complexity of real star formation histories, but continuous refinement and validation of our methods could eventually bring us ever so close.

"One must imagine Sisyphus happy."

Acknowledgements

I would like to thank the people without whom this project would not have been possible. My supervisors, Prof. Karina Caputi and Dr. Edoardo Iani, have provided invaluable guidance that helped me navigate through this thesis. Karina's overarching vision and insightful feedback were instrumental in shaping the direction of my research, while Edoardo's willingness to schedule a two-hour meeting to discuss a graph that we did not even include is a testament to the level of his dedication and support.

I also extend my gratitude to the other members of our research team for their insightful input, giving me a broader perspective on my work.

Finally, I am grateful to my peers, friends and family. Your examples of excellence have inspired me throughout this journey, while also providing a vital balance and helping me maintain clear judgement.

Even though I am the sole author of this thesis, the use of "we" throughout this work reflects the collective support, collaboration, and encouragement that I have received from all of you. Without it, this work would not exist.

Facilities: HST, JWST, VLT

Software: Astropy (Astropy Collaboration et al. 2013, 2018, 2022), CIGALE (Boquien et al. 2019), Matplotlib (Hunter 2007), NumPy (Harris et al. 2020), Pandas (The pandas development Team 2024), SciPy (Virtanen et al. 2020).

APPENDIX

A. COMPARISON WITH IANI ET AL. 2024

Throughout this work, we have referred much to Iani (2024). Apart from being a source of our LAE sample, that work has performed a similar SED fit for these objects using LePHARE (Ilbert et al. 2006), and here we discuss the extent to which our results match. In their fitting an exponential SFH was assumed, therefore in Figure 9 we compare the of age, stellar mass, SFR and E(B-V) obtained in that paper and and our outputs for the same SFH.

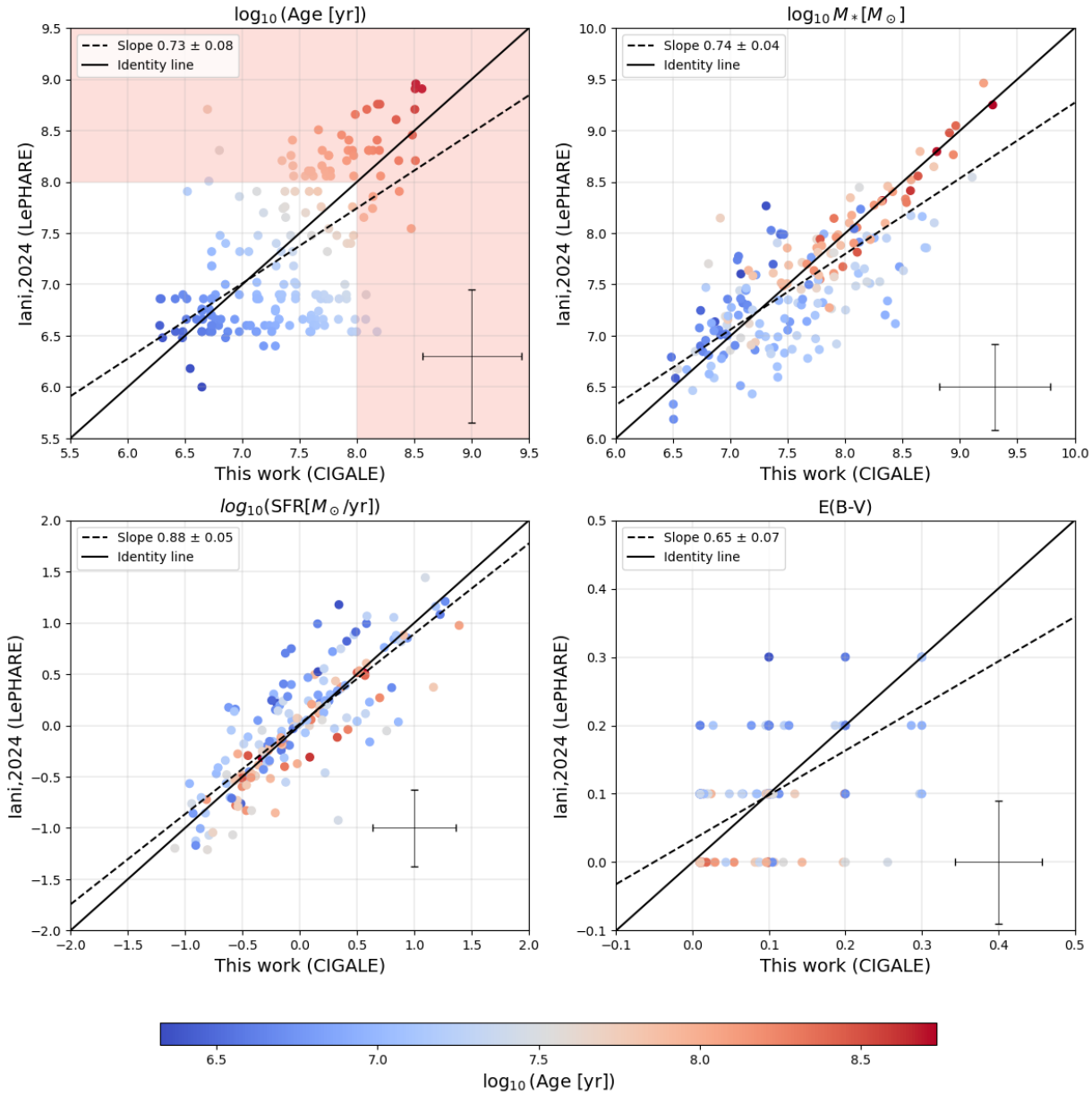

Figure 9: Comparison of our exponential SFH outputs with ones from Iani (2024). The figure follows the same general conventions as other figures in this paper.

The star formation rates show the highest correlation; however, just as we used a Kennicutt approximation in order to avoid unreliable star formation rates from the SED fit, Iani et al. determined the SFRs though an empirically

estimated UV continuum slope (for most objects). Since both methods trace the same stellar population of rest frame UV emitters, we expectedly find them to be in good agreement. The thickness of scatter is most likely caused by E(B-V) discrepancy, as dust correction is performed for both SFR estimations.

We identify two main reasons for possible discrepancies in E(B-V). The first is discretization, as LePHARE pre-computes all models on a grid before choosing the best fitting one. On top of that, although Bayesian estimation is an option in CIGALE, it was not considered for dust attenuation, resulting in both datasets being heavily binned thereby complicating the quality comparison. Then, the disagreement could be caused by the age-dust degeneracy; since both the age and E(B-V) distributions are rich in outliers, we cannot exclude the possibility of contamination.

Interestingly enough, we find that both CIGALE and LePHARE agree well on the stellar mass of older objects, as can be seen by a distinct tail of old galaxies along the identity line in the stellar mass panel. On the contrary, among the masses of young LAEs we observe a considerable scatter with a slight trend for overestimation in CIGALE. Figure 7 in Pacifici et al. (2023) shows a comparison of masses obtained using both LePHARE and CIGALE for a sample at $z \approx 3$, and finds no significant discrepancy between the codes. However, the masses considered in their analysis were all in the $10^{8-10} M_{\odot}$ range, corroborating our observations for old LAE correlation but giving no information about low-mass systems. Perhaps, a similar study with a wider range would shed more light on this behavior.

Overall, we believe the obtained results are satisfactorily similar. General trends are consistent between the two codes, and the scatter is mostly within 0.3 dex of the best-fit line. Still, future studies with larger and more diverse samples would be required to refine our understanding of younger and less massive galaxies such as Ly-α emitters.

REFERENCES

Arrabal Haro, P., Rodríguez Espinosa, J. M., Muñoz-Tuñón, C., et al. 2020, MNRAS, 495, 1807. doi:10.1093/mnras/staa1196

Astropy Collaboration, Robitaille, T. P., Tollerud, E. J., et al. 2013, A&A, 558, A33. doi:10.1051/0004-6361/201322068

Astropy Collaboration, Price-Whelan, A. M., Sipőcz, B. M., et al. 2018, AJ, 156, 123. doi:10.3847/1538-3881/aabc4f

Astropy Collaboration, Price-Whelan, A. M., Lim, P. L., et al. 2022, ApJ, 935, 167. doi:10.3847/1538-4357/ac7c74

Bacon, R., Accardo, M., Adjali, L., et al. 2010, Proc. SPIE, 7735, 773508. doi: 10.1117/12.856027

Bacon, R., Brinchmann, J., Conseil, S., et al. 2023, A&A, 670, A4. doi: 10.1051/0004-6361/202244187

Bagley, M. B., Finkelstein, S. L., Koekemoer, A. M., et al. 2023, ApJL, 946, L12. 10.3847/2041-8213/acbb08

Bertin, E. & Arnouts, S. 1996, A&AS, 117, 393. doi: 10.1051/aas:1996164

Bisigello, L., Caputi, K. I., Grogin, N., et al. 2018, A&A, 609, A82. doi: 10.1051/0004-6361/201731399

Boquien, M., Buat, V., & Perret, V. 2014, A&A, 571, A72. doi: 10.1051/0004-6361/201424441

Boquien, M., Burgarella, D., Roehlly, Y., et al. 2019, A&A, 622, A103. doi: 10.1051/0004-6361/201834156

Boquien, Médéric. Personal communication. June 21, 2024.

Bruzual, G. & Charlot, S. 2003, MNRAS, 344, 1000. doi: 10.1046/j.1365-8711.2003.06897.x

Buat, V., Marcillac, D., Burgarella, D., et al. 2007, A&A, 469, 19. doi: 10.1051/0004-6361:20066685

Calzetti, D., Kinney, A. L., & Storchi-Bergmann, T. 1994, ApJ, 429, 582. doi: 10.1086/174346

Calzetti, D., Armus, L., Bohlin, R. C., et al. 2000, ApJ, 533, 682. doi: 10.1086/308692

Calzetti, D. 2013, Secular Evolution of Galaxies, 419. doi: 10.48550/arXiv.1208.2997

Caputi, K. I., Caminha, G. B., Fujimoto, S., et al. 2021, ApJ, 908, 146. doi: 10.3847/1538-4357/abd4d0

Caputi, K. I., Deshmukh, S., Ashby, M. L. N., et al. 2017, ApJ, 849, 45. doi: 10.3847/1538-4357/aa901e

Carnall, A. C., Leja, J., Johnson, B. D., et al. 2019, ApJ, 873, 44. doi: 10.3847/1538-4357/ab04a2

Chabrier, G. 2003, PASP, 115, 763. doi:10.1086/376392

Conroy, C. 2013, ARA&A, 51, 393. doi:10.1146/annurev-astro-082812-141017

da Cunha, E., Charlot, S., & Elbaz, D. 2008, MNRAS, 388, 1595. doi:10.1111/j.1365-2966.2008.13535.x

da Cunha, E., Walter, F., Smail, I. R., et al. 2015, ApJ, 806, 110. doi:10.1088/0004-637X/806/1/110

Dunlop, J. S., Cirasuolo, M., & McLure, R. J. 2007, MNRAS, 376, 1054. doi:10.1111/j.1365-2966.2007.11453.x

Evans, I. N., Primini, F. A., Miller, J. B., et al. 2020, AAS Meeting Abstracts

Finkelstein, S. L., Rhoads, J. E., Malhotra, S., et al. 2009, ApJ, 691, 465. doi:10.1088/0004-637X/691/1/465

Finkelstein, S. L., Hill, G. J., Gebhardt, K., et al. 2011, ApJ, 729, 140. doi:10.1088/0004-637X/729/2/140

Finkelstein, S. L. 2016, PASA, 33, e037. doi:10.1017/pasa.2016.26

Harris, C. R., Millman, K. J., van der Walt, S. J., et al. 2020, Nature, 585, 357. doi:10.1038/s41586-020-2649-2

Haskell, P., Das, S., Smith, D. J. B., et al. 2024, MNRAS, 530, L7. doi:10.1093/mnrasl/slae019

Haskell, P., Smith, D. J. B., Cochrane, R. K., et al. 2023, MNRAS, 525, 1535. doi:10.1093/mnras/stad2315

Hunt, L. K., De Looze, I., Boquien, M., et al. 2019, A&A, 621, A51. doi:10.1051/0004-6361/201834212

Hunter, J. D. 2007, Computing in Science and Engineering, 9, 90. doi:10.1109/MCSE.2007.55

Iani, E., Caputi, K. I., Rinaldi, P., et al. 2024, ApJ, 963, 97. doi:10.3847/1538-4357/ad15f6

Ilbert, O., Arnouts, S., McCracken, H. J., et al. 2006, A&A, 457, 841. doi:10.1051/0004-6361:20065138

Illingworth, G. D., Magee, D., Oesch, P. A., et al. 2013, ApJS, 209, 6.
doi:10.1088/0067-0049/209/1/6

Kennicutt, R. C. & Evans, N. J. 2012, ARA&A, 50, 531.
doi:10.1146/annurev-astro-081811-125610

Kennicutt, R. C. 1998, ARA&A, 36, 189.
doi:10.1146/annurev.astro.36.1.189

Lehnert, M. D., van Driel, W., Le Tiran, L., et al. 2015, A&A, 577, A112.
doi: 10.1051/0004-6361/201322630

Leja, J., Carnall, A. C., Johnson, B. D., et al. 2019, ApJ, 876, 3.
doi: 10.3847/1538-4357/ab133c

Luo, B., Brandt, W. N., Xue, Y. Q., et al. 2017, ApJS, 228, 2.
doi: 10.3847/1538-4365/228/1/2

Lyu, J., Alberts, S., Rieke, G. H., et al. 2022, ApJ, 941, 191.
doi: 10.3847/1538-4357/ac9e5d

Madau, P. & Dickinson, M. 2014, ARA&A, 52, 415.
doi:10.1146/annurev-astro-081811-125615

Maraston, C., Pforr, J., Renzini, A., et al. 2010, MNRAS, 407, 830.
doi:10.1111/j.1365-2966.2010.16973.x

Merlin, E., Fontana, A., Castellano, M., et al. 2018, MNRAS, 473, 2098.
doi:10.1093/mnras/stx2385

Navarro-Carrera, R., 2024, in preparation.

Ning, Y., Cai, Z., Lin, X., et al. 2024, ApJL, 963, L38.
doi: 10.3847/2041-8213/ad292f

Noeske, K. G., Weiner, B. J., Faber, S. M., et al. 2007, ApJL, 660, L43.
doi: 10.1086/517926

Oesch, P. A., Brammer, G., Naidu, R. P., et al. 2023, MNRAS, 525, 2864.
doi: 10.1093/mnras/stad2411

Oke, J. B. & Gunn, J. E. 1983, ApJ, 266, 713.
doi: 10.1086/160817

Ono, Y., Ouchi, M., Shimasaku, K., et al. 2010, ApJ, 724, 1524.
doi: 10.1088/0004-637X/724/2/1524

Ouchi, M., Ono, Y., & Shibuya, T. 2020, ARA&A, 58, 617.
doi: 10.1146/annurev-astro-032620-021859

Pacifici, C., da Cunha, E., Charlot, S., et al. 2015, MNRAS, 447, 786.
doi: 10.1093/mnras/stu2447

Pacifici, C., Iyer, K. G., Mobasher, B., et al. 2023, ApJ, 944, 141.
doi: 10.3847/1538-4357/acacff

Papovich, C., Cole, J. W., Yang, G., et al. 2023, ApJL, 949, L18.
doi: 10.3847/2041-8213/acc948

Pérez-González, P. G., Barro, G., Rieke, G. H., et al. 2024, ApJ, 968, 4.
doi: 10.3847/1538-4357/ad38bb

Ranalli, P., Comastri, A., Vignali, C., et al. 2013, A&A, 555, A42.
doi: 10.1051/0004-6361/201321211

Reddy, N. A., Pettini, M., Steidel, C. C., et al. 2012, ApJ, 754, 25.
doi: 10.1088/0004-637X/754/1/25

Rieke, M. J., Robertson, B., Tacchella, S., et al. 2023, ApJS, 269, 16.
doi: 10.3847/1538-4365/acf44d

Rinaldi, P., Caputi, K. I., van Mierlo, S. E., et al. 2022, ApJ, 930, 128.
doi: 10.3847/1538-4357/ac5d39

Rinaldi, P., Navarro-Carrera, R., Caputi, K. I., et al. 2024, arXiv:2406.13554.
doi: 10.48550/arXiv.2406.13554

Rodrigo, C. & Solano, E. 2020, XIV.0 Scientific Meeting (virtual) of the Spanish Astronomical Society, 182

Rosani, G., Caminha, G. B., Caputi, K. I., et al. 2020, A&A, 633, A159.
doi: 10.1051/0004-6361/201935782

Salpeter, E. E. 1955, ApJ, 121, 161.
doi: 10.1086/145971

Schawinski, K., Thomas, D., Sarzi, M., et al. 2007, MNRAS, 382, 1415.
doi:10.1111/j.1365-2966.2007.12487.x

Schwarz, G. 1978, The Annals of Statistics, 6, 461.
doi:10.1214/aos/1176344136

Simha, V., Weinberg, D. H., Conroy, C., et al. 2014, arXiv:1404.0402.
doi: 10.48550/arXiv.1404.0402

Soderblom, D. R., Hillenbrand, L. A., Jeffries, R. D., et al. 2014, Protostars and Planets VI, 219.
doi: 10.2458/azu_uapress_9780816531240-ch010

Sonnett, S., Meech, K., Jedicke, R., et al. 2013, PASP, 125, 456.
doi: 10.1086/670593

Sparre, M., Hayward, C. C., Feldmann, R., et al. 2017, MNRAS, 466, 88.
doi: 10.1093/mnras/stw3011

Sparre, M., Hayward, C. C., Springel, V., et al. 2015, MNRAS, 447, 3548.
doi: 10.1093/mnras/stu2713

Speagle, J. S., Steinhardt, C. L., Capak, P. L., et al. 2014, ApJS, 214, 15.
doi: 10.1088/0067-0049/214/2/15

Springel, V., Pakmor, R., Pillepich, A., et al. 2018, MNRAS, 475, 676.
doi: 10.1093/mnras/stx3304

The pandas development Team 2024, Zenodo
doi: 10.5281/zenodo.3509134

Tilvi, V., Pirzkal, N., Malhotra, S., et al. 2016, ApJL, 827, L14.
doi: 10.3847/2041-8205/827/1/L14

Virtanen, P., Gommers, R., Oliphant, T. E., et al. 2020, Nature Methods, 17, 261.
doi: 10.1038/s41592-019-0686-2

Whitaker, K. E., Ashas, M., Illingworth, G., et al. 2019, ApJS, 244, 16.
doi: 10.3847/1538-4365/ab3853

Whitaker, K. E., Labbé, I., van Dokkum, P. G., et al. 2011, ApJ, 735, 86.
doi: 10.1088/0004-637X/735/2/86

Williams, C. C., Tacchella, S., Maseda, M. V., et al. 2023, ApJS, 268, 64
doi: 10.3847/1538-4365/acf130

Withers, S., Muzzin, A., Ravindranath, S., et al. 2023, ApJL, 958, L14.
doi: 10.3847/2041-8213/ad01c0

Yuan, T.-T., Kewley, L. J., & Richard, J. 2013, ApJ, 763, 9.
doi: 10.1088/0004-637X/763/1/9